ICONHIC2022
3rd International Conference on Natural Hazards & Infrastructure
5-7 July 2022, Athens, Greece

Parametric Study on Natural Rubber based Low-Cost Base Isolation Technique for Masonry Buildings

Zoheb Nawaz Md, M.Tech[1], Mohan S C, Ph.D[2]
[1,2] *Department of Civil Engineering, BITS Pilani Hyderabad Campus, Hyderabad-500078, Telangana, India*

Kalyana Rama J S, Ph.D[3]
[3] *Department of Civil Engineering, Ecole Centrale School of Engineering, Mahindra University, Hyderabad-500043, Telangana, India.*

ABSTRACT

In developing countries, masonry is widely used for construction due to its availability and low cost. The masonry buildings are vulnerable to moderate and severe earthquakes due to their brittle nature. The use of base isolation techniques for masonry building has seen an increasing trend in the past two decades. However, existing isolation techniques are uneconomical, requiring skilled labor and specialized manufacturing processes. Hence, the present study focuses on developing a novel low-cost base isolation technique using locally available natural rubber. In the proposed technique, unbonded rubber is spread beneath the plinth level of the wall. A parametric study has been conducted numerically to evaluate the isolation efficiency of the rubber with varying thicknesses and lengths. This study also involves different sizes and thicknesses of the rubber placed intermittently with gaps. ABAQUS CAE V6.13 is used for simulating the behavior of natural rubber and masonry building. The properties of the rubber and its numerical modeling has been validated with the existing literature and further used for parametric study. From the parametric study, suitable dimensions and thickness of the rubber are obtained to increase the performance of the proposed isolation technique without sliding. The identified rubber dimensions placed intermittently with gaps have led to increased vertical stiffness and damping with required low horizontal stiffness compared to rubber spread throughout the plinth.

Keywords: Base isolation, masonry buildings, low-cost, natural rubber, regression analysis

INTRODUCTION

Numerous studies have focused on earthquake resistance strategies for residential structures. (Minke, 1984) Today, these technologies are only applicable in a limited number of cases as those are not feasible or uneconomical. Most buildings in developing regions remain vulnerable to the effects of an earthquake, as many of them are built using current practices without seismic provisions. As a result, the development of novel and low-cost seismic isolation systems can have a significant impact on seismically active areas, particularly in developing countries. The development of more affordable technologies (Sierra et al, 2019a) may encourage the use of base-isolation systems in new and existing structures, thereby increasing the seismic resistance of residential buildings in developing regions of the world. Numerous studies have established the superiority of fibre-reinforced elastomeric bearings (FREIs) over traditional steel-reinforced elastomeric bearings (SREIs) (Karimzadeh et al, 2014; Kelly, 1999; Sierra et al, 2019). Although research has been devoted to experimental (Russo and Pauletta, 2013; Spizzuoco et al, 2014; Toopchi-Nezhad et al, 2008a, 2008b), analytical (Russo et al, 2013; Toopchi-Nezhad, 2014), and numerical (Osgooei et al, 2014; Toopchi-Nezhad et al, 2011; Vaiana et al, 2019; Van Engelen et al, 2015) modeling of their complex mechanical performance,

[1] e-mail: p20180415@hyderabad.bits-pilani.ac.in, [2] mohansc@hyderabad.bits-pilani.ac.in,
[3]srikalyanarama.j@mahindrauniversity.edu.in

further examinations of this technology are required as long as a significant validation of the expected behavior of FREIs is lacking.

There are few studies in the literature on the application of FREI to masonry structures. Several of them conducted experimental studies to demonstrate the efficacy of FREI in masonry (Das et al, 2016a). Few researchers have developed numerical methods for validating it (Das et al, 2016b; Habieb et al, 2018; Thuyet et al, 2018). Unlike other engineered structures, masonry requires an additional plinth or slab to prevent differential settlements, which adds cost and makes FREI less economical for masonry (Tran et al, 2020). While these studies established the efficacy of FREI, individual studies proposed other isolation techniques. Among these are sliding mechanisms made of various materials (Nanda et al, 2016), pebble stone layer isolation (Banović et al, 2019), scrap tire pads (Mishra et al, 2013; Turer and Özden, 2008), rubber soil mixture (Forcellini, 2020), sand rubber deformable granular (Tsiavos et al, 2019), and PVC sandwich system (Tsiavos et al, 2020). While some attempts have been made to reduce the seismic response of masonry buildings, none of these techniques is viable because the sliding system lacks a re-centring mechanism, causing permanent horizontal displacement, and the rubber sand mixtures technique necessitates cumbersome work, making it less cost-effective. As a result, new low-cost seismic isolation systems may significantly impact earthquake-prone areas, particularly in developing countries. Low-cost techniques may encourage using base isolation systems to strengthen structures against earthquakes. This study aims to develop a novel low-cost base isolation technique that a layperson can easily adopt.

The present study demonstrates the effectiveness of the proposed low-cost novel base isolator for unreinforced masonry buildings. Initially, the length of the rubber is obtained by conducting simulation trials. After a thorough calibration process, the optimal properties of the rubber are presented. The results of nonlinear time-history analyses are described to show that the proposed base isolator configuration has better seismic behavior than the fixed-base configuration. This research provides a basis for future developments in the proposed area, which will aid in reducing the seismic risk of masonry buildings in developing countries like India.

PRELIMINARY ANALYSIS

An initial trial simulation is performed to investigate the suitability of unreinforced natural rubber as an isolator for masonry buildings. The numerical simulation is carried out with the help of commercially available finite element software, ABAQUS CAE-6.13. A rubber layer of 25mm thickness is provided throughout the length of the plinth beam. Like the FREI's for masonry application, an additional plinth is modeled between the rubber layer and the walls (Tran et al, 2020). As shown in Figure 1, the rubber is sandwiched between the two beams.

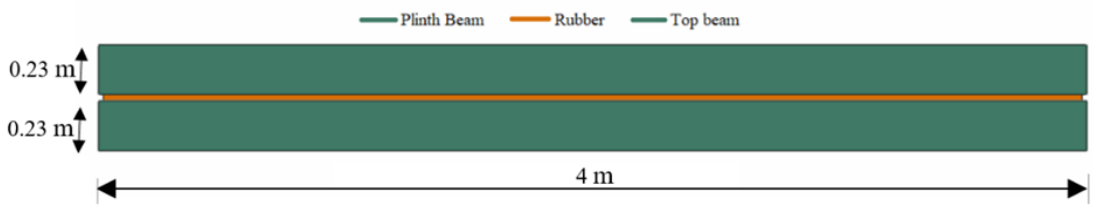

Figure 1. *Continuous rubber-beam model*

To bring computational efficiency during parametric study, the load from the masonry wall is applied on plinth beam instead of modelling the wall, without compromising the isolator behavior. The frictional coefficients used for the contact between the top beam and rubber, rubber, and plinth beam are 1.00 and 0.85, respectively (*Coefficient of Friction Equation and Table Chart - Engineers Edge*, n.d.). At the bottom of the plinth, all degrees of freedom are constrained. The top beam is subjected to a displacement amplitude of 25mm with a frequency of 0.5 Hz in the longitudinal direction. The beams are assigned with an 8-noded hexahedron element, and the same element with the hybrid formulation is assigned to rubber for nonlinear deformation. There are a total of 4152 elements and 8446 nodes for the rubber-beam model. Sliding is observed between the lower beam and the rubber as a result of the rubber's higher horizontal stiffness. According to the literature, the isolator's horizontal stiffness should be reduced. However, by using rubber throughout, the horizontal stiffness is increased, making isolation less effective. One method for making the rubber more flexible is to drill holes horizontally down the length of the rubber (Tran et al, 2020). Because the thickness considered for this technique is relatively thin, this approach is not feasible. Figure 3 depicts the force-displacement response of the continuous rubber beam model, with the curve reaching its maximum force of 57kN at a displacement of

5mm. The force generated by horizontal displacement has overcome the frictional force after 5mm, and sliding occurs for the remaining 20mm of displacement. This sliding is caused by the continuous rubber's higher horizontal stiffness, which is 2.34 kN/m. To reduce the horizontal stiffness, an intermittent rubber-beam model is used in the simulation, with a gap at increasing 100mm intervals at the centre of the rubber-beam model, as shown in Figure 2.

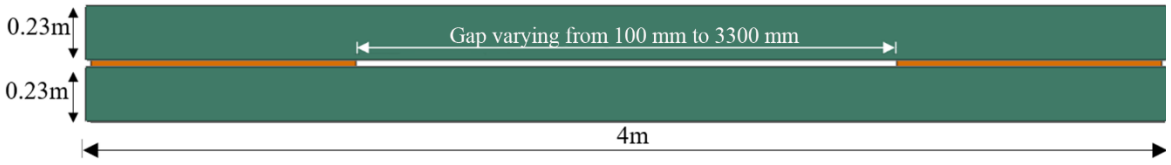

Figure 2. *Intermittent rubber-beam model*

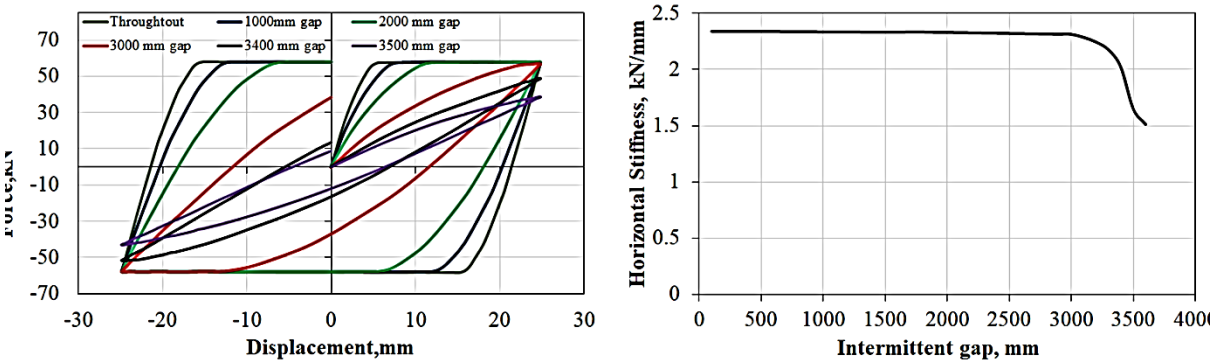

Figure 3. *(a) Force-displacement curve of continuous rubber-beam model and intermittent rubber-beam model with different gaps, (b) variation of horizontal stiffness with increase in intermittent gap.*

Figure 3 depicts the hysteresis curve of the intermittent rubber-beam model with every 1000 mm gap to distinguish the curves. As the gap increases to 3000mm, the sliding displacement decreases due to a decrease in horizontal stiffness. When a 3000mm gap in rubber is provided, there is no sliding in the positive direction, but sliding can be seen in the negative direction. At the same load, the sliding is caused by the transition from static to kinetic friction (*6.2 Friction – University Physics Volume 1*, n.d.). Figure 3(b) shows that until 3000mm intermittent gap, the horizontal stiffness is approximately constant, i.e., 2.3kN/mm, and then there is a significant reduction in the horizontal stiffness. When the gap reached 3400mm and 3500mm, the horizontal stiffness decreased significantly, and no sliding is observed. This response is also depicted in Figure 3. The horizontal stiffness produced by these two models is 1.65kN/mm and 1.58kN/mm, respectively.

The simulation shows that if the length of each rubber is between 150mm and 250mm, the model produces satisfactory results in terms of horizontal stiffness, and these rubber lengths are used to optimize the behaviour of the proposed technique. The above simulation is carried out using natural rubber properties tabulated in Table 1.

Table 1. *Hyperelastic Properties of Rubber*

Rubber Properties	**C10**	**C20**	**C30**	**D1**
	9.20E-02	-9.51E-04	1.74E-05	1.09E-03

REGRESSION ANALYSIS

There are different parameters of rubber that affect its behavior. Among them, crucial ones are rubber dimensions, shear modulus of rubber, temperature, and strain rate. In this study, only the dimension of rubber has been considered as input. To conduct regression analysis, a fully factorial design approach is used. Each factor is treated as a parameter in this approach, and three levels are fixed, namely low, medium, and high. Table 2 lists the parameters and their levels. The total nine (3^2) number of combinations generated as listed in Table 3, when the factors are taken into account (Dezfuli and Alam, 2013).

Table 2. *Factors and its levels*

Factor	Symbol	Level		
		1	**2**	**3**
l_r	A	150	200	250
t_r	B	12.5	25	50

In the regression analysis, the length(l_r), and thickness(t_r), of rubber are denoted by A, and B respectively. The first order (A, and B), second-order (A^2, and B^2) and interaction (AB) effects are considered to model the behaviour accurately. All 9 simulations are conducted in ABAQUS, and the response is quantified in terms of vertical stiffness(K_V), horizontal stiffness (K_H) and equivalent viscous damping (β). These responses are used as output for the regression analysis. Table 4 summarises the response output simulated and obtained in ABAQUS for each alternative.

Table 3. *A three-factorial design consisting of three levels and two factors*

Run	Factor	
	A	**B**
1	250	50
2	200	50
3	150	50
4	250	25
5	200	25
6	150	25
7	250	12.5
8	200	12.5
9	150	12.5

Table 4. *Output of rubber isolator in a factorial design*

Run	Output		
	K_V **(kN/mm)**	K_H **(kN/mm)**	**β** (%)
1	12.25	0.97	2.77
2	18.29	1.32	3.07
3	24.80	1.64	4.21
4	57.14	1.71	8.10
5	91.09	2.11	11.11
6	127.78	2.19	17.95
7	282.21	2.21	24.09
8	455.45	2.31	30.98
9	621.62	2.32	37.53

The output parameters cannot be obtained directly from ABAQUS. After each simulation on rubber-beam models, the following equations are used to determine the output parameters. The vertical stiffness (K_V) of the rubber can be determined as,

$$K_V = \frac{w}{\Delta_v} \tag{1}$$

where *w* denotes the total load acting the rubber and Δ_v denotes the vertical displacement of rubber. The rubber isolator's effective horizontal stiffness can be determined as,

$$K_H = \frac{F_{max} - F_{min}}{\Delta_{max} - \Delta_{min}} \tag{2}$$

where F_{max} and F_{min} denotes the maximum shear forces in a positive and negative direction, respectively. Δ_{max} and Δ_{min} denote the maximum displacements in the positive and negative directions. The equivalent viscous damping coefficient of the isolator can be calculated as,

$$\beta = \frac{W_d}{2\pi K_H {\Delta_{max}}^2} \tag{3}$$

where W_d is the area within the hysteresis curve derived from the shear force-displacement curve.

Figure 4 illustrates the process of determining the rubber's response when the two factors are taken into account. In Figure 5, the normalized output is compared amongst each alternative in accordance with the arrangement shown in Table 3. Normalized values are calculated by dividing each response output by the sum of all the responses in the corresponding column. Table 4 lists the output parameters of the rubber isolator. These simulations show that after the sixth iteration, sliding occurs in the intermittent rubber-beam model between the rubber and the plinth beam. The main reason for the sliding is due to an increase of horizontal stiffness with reduction in rubber thickness. As the sliding causes recentering issues in the building, the last three alternatives are omitted from the regression model generation. If these alternatives are considered when developing a regression model, the model will produce incorrect results.

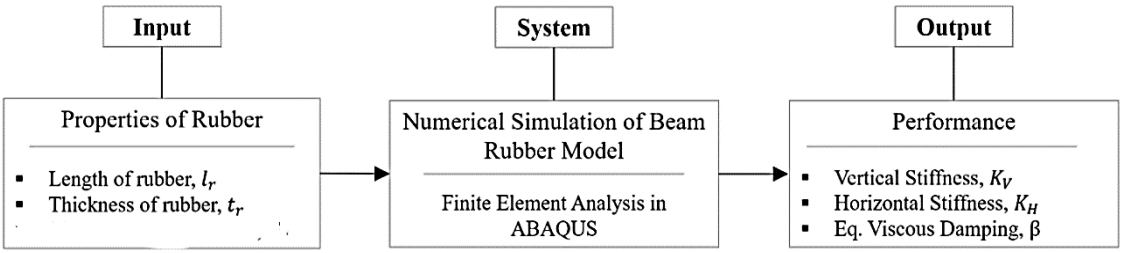

Figure 4. *Procedure to determine the output*

The significance level for measuring the output response (stiffness or damping of rubber) can be determined by dividing the coefficient of the factor by its standard error. The regression toolbox in Excel is used to obtain the coefficient and t-statistic values for each factor. The coefficients are included for the main effects (A, B, and C) and second-order and interaction effects ($A^2, B^2, C^2, AB, BC, CA$, and ABC). Table 5 summarizes these values.

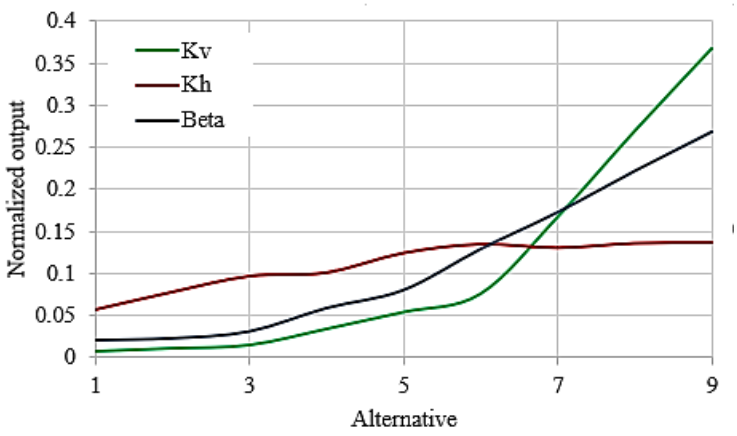

Figure 5. *Normalized output for different alternatives*

Table 5. *Each response's coefficient in the regression model*

Effect	K_V **(kN/mm)**		K_H **(kN/mm)**		**β** (%)	
	Coeff.	***t Stat***	***Coeff.***	***t Stat***	***Coeff.***	***t Stat***
Intercept	-51.17	5.62	0.23	0.31	7.98	0.67
A	1.16	12.42	0.01	1.99	-0.0040	0.03
B	0.00	0.00	0.00	0.00	0.00	0.00
A^2	0.00032	1.41	-0.000025	1.39	0.00047	1.56
B^2	0.02	15.90	-0.00050	4.34	0.0041	2.21
AB	-0.02	44.23	0.000041	0.97	-0.0034	4.87

By comparing anticipated responses derived from regression models to actual values obtained through numerical simulations and utilizing the t-statistic for each coefficient, the following simplified regression models are proposed for each response: Equation 4, 5, and 6.

$$K_V = -51.17 + 1.16A + 0.00032A^2 + 0.02B^2 - 0.02AB \text{ (kN/mm)} \quad (4)$$

$$K_h = 0.23 + 0.01A - 0.000025\,A^2 - 0.00050B^2 + 0.000041AB \text{ (kN/mm)} \quad (5)$$

$$\beta = 7.98 - 0.0040A + 0.00047A^2 + 0.0041B^2 - 0.0034AB \quad (6)$$

where A and B are the length of rubber layers (l_r), and the thickness of rubber (t_r) respectively.

There are numerous criteria (C_j) and alternatives (A_i) in any case of the multi-criteria problem. The problem's primary objective is to maximize, minimize, or calibrate the criterion between the various alternatives. Optimization of the problem is only possible if it produces the criteria under optimal conditions. Different weighing and scoring methods can be used to categorize the alternatives. To begin, each attribute must be assigned a weightage. Secondly, a score is generated for each alternative based on the weightage (Hwang and Masud, 1979). There are several different scoring methods. The weighted sum method and TOPSIS are the most frequently used techniques. Among them (Yoon and Hwang, 1995) the best alternative is the one that yields the highest score, whereas the worst alternative has the least score.

The first step in optimization is to transform the attributes into "highest, the best" or "lowest, the best" conditions. For instance, if one criterion (C_x) must be maximized while other criteria must be minimized; the inverse of C_x results in the goal of minimizing all criteria. Due to the fact that the scale and units of all attributes cannot be identical, normalization techniques can be used.

The alternative's score is defined by the following equation using the Weighter score method.

$$S_i = \sum_{j=1}^{n} \widehat{W}_j \hat{C}_{ij} \quad (7)$$

Where $\widehat{W}_j$is the normalized weightage for the criterion j and $\hat{C}_{ij}$ is the normalized criterion j for alternative i, and n is the total number of criteria.

In this study, six previously defined combinations are chosen as alternatives, and three output responses are assigned as criteria. Vertical stiffness should be greater than horizontal stiffness, and the equivalent damping ratio should be maximum for effective energy dissipation in any base isolation system. Thus, horizontal stiffness should be minimized in this case, while vertical stiffness and damping ratio should be maximized. To ensure that the problem's objective maximizes all criteria, the horizontal stiffness of each of the six alternatives is inversed. Following that, the score can be evaluated using the ranking system "the higher, the better." Figure 6 illustrates the entire process of optimizing the rubber parameters.

The score of each alternative can be defined in Equation 8

$$S_i = \widehat{W_1}\widehat{K_{V_i}} + \widehat{W_2}\widehat{K_{H_i}}' + \widehat{W_3}\hat{\beta} \quad (8)$$

Where $\widehat{W_1}, \widehat{W_2}, \widehat{W_3}$ are the normalized weights corresponding to their criteria. $\widehat{K_{V_i}}$ is the normalized vertical stiffness, $\widehat{K_{H_i}}'$ is the normalized horizontal stiffness and $\hat{\beta}$ is the normalized equivalent viscous damping.

After inverting the effective horizontal stiffness ($\widehat{K_{H_i}}'$) and normalizing all criteria for each alternative the score for each case, S_i is calculated using the normalized weights of each criterion given in Table 6 using the weighted score method (9).

Table 6. *Normalized weight assigned to criterion* (Dezfuli and Alam, 2013)

Criterion	**Weight**
Vertical Stiffness	0.18
Horizontal Stiffness	0.39
Damping Coefficient	0.43

The optimal rubber properties are determined by ranking the alternatives in order of increasing to decreasing scores. Table 8 summarizes the four best alternatives.

$$S_i = 0.18\widehat{K_{V_i}} + 0.39\widehat{K_{H_i}}' + 0.43\hat{\beta} \quad (1)$$

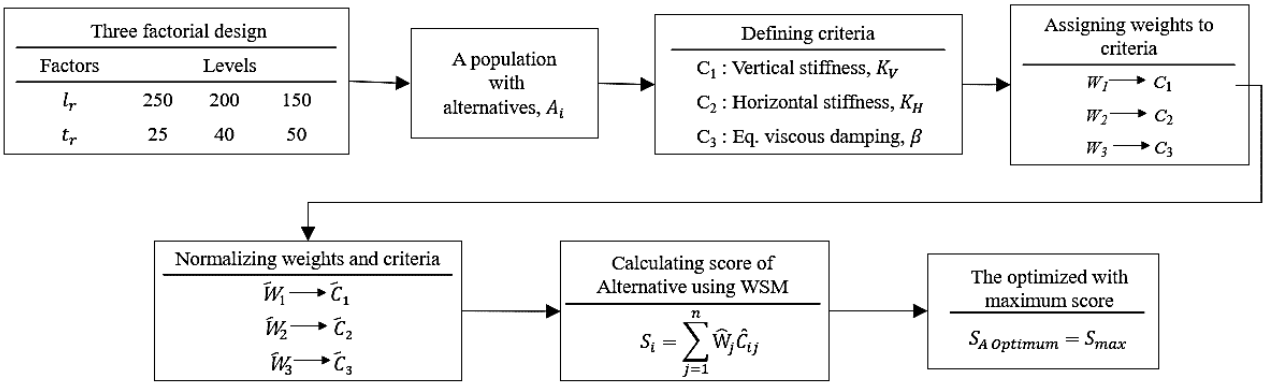

Figure 6. *Flow chart of Multi-criteria optimization*

Table 7 *Characteristics of 1st to 3rd ranked rubber*

Rank				Stiffness		Damping
	ID	l_r (mm)	t_r (mm)	K_V (kN/mm)	K_H (kN/mm)	β (%)
1st	A6	250	25	127.8	2.29	17.95
2nd	A5	200	25	91.1	2.11	11.11
3rd	A4	150	25	57.1	1.71	8.10

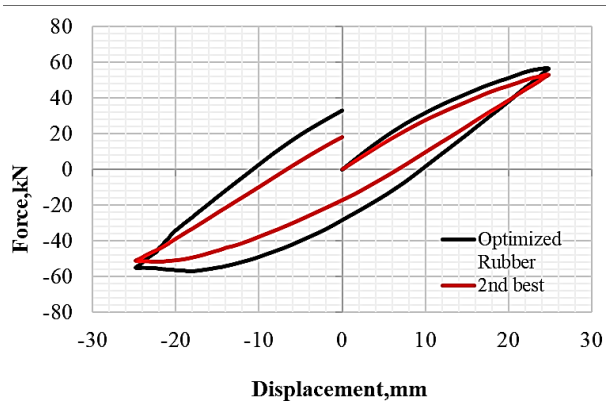

Figure 7. *Force-Displacement curve of Optimized and 2nd best Rubber*

According to this ranking, the optimized rubber should have a length of 250mm and a thickness of 25mm. In Figure 7, the lateral force-displacement hysteresis curves for the optimized and second-best rubbers are plotted for an applied load of 0.057Mpa vertical pressure and cyclic lateral displacement of 25mm at a frequency of 0.5 Hz.

APPLICATION OF OPTIMIZED RUBBER ISOLATOR FOR MASONRY BUILDING

A small one-story masonry structure is analyzed using rubber isolator's optimized parameters to determine its effectiveness. Under quasi-static loading, the building is tested experimentally (Shahzada et al., 2012). The building measures 4.12m X 3.96m in plan and has a wall thickness of 230mm. On the top of the door and windows, a lintel is installed. The roof of the building is a reinforced slab with a thickness of 150mm. A parapet wall with a thickness of 340mm is provided on top of the slab. The building's plan and elevation are depicted in Figure 8. The dimensions of the walls and openings are listed in Table 8.

Table 8. *Geometry of masonry buildings including openings*

Description	Dimension	Description	Dimension
Wall 1, 2	0.99 m × 3.35 m	Door	1.68 m × 2.59 m
Wall 3, 4	1.14 m × 3.35 m	Window 1	0.8 m × 1.68 m
Wall 5, 6, 7	0.686 m × 3.35 m	Window 2	1.22 m × 1.68 m
Wall 8	0.3.51 m × 3.35 m	-	-

Tables 9 summarise the physical and mechanical properties of the masonry building as determined by (Shahzada et al., 2012). The properties of the same masonry building modelled using concrete damage plasticity (Choudhury et al, 2015) and are tabulated in Table 10. These properties are used in this study for numerical simulation using ABAQUS.

Table 9. *Mechanical Properties of Material used in Modelling* (Shahzada et al, 2012)

S.No.	Property	Value
01	Masonry Compressive Strength	3.05 Mpa
02	Masonry Tensile Strength	0.05 Mpa
03	Elastic Modulus of Masonry	1227 Mpa
04	Poisson's Ratio	0.15
05	Density of Masonry	1495 kg/m^3
06	Elastic Modulus of Concrete	25000 Mpa
07	Poisson’s Ratio	0.2
08	Density of Concrete	2400 Mpa

The numerical model of the masonry building is used for pushover analysis. The obtained pushover curve is compared with experimental results [36]. As shown in Figure 9, the results of the analysis are in good agreement with the experimentally obtained values. The maximum load-carrying capacity of the masonry building determined by experimental testing is 106.7kN and 105kN by numerical simulation. Furthermore, as shown in Figure 10, the observed damage patterns from this study are consistent with those found in the existing literature (Choudhury et al, 2015). As the experimental and numerical results agreed so well, the simulation is expanded to assess the response of the masonry building with optimized rubber isolator.

Table 10. *Concrete Damage Plasticity Properties* (Choudhury et al, 2015)

Dilatation angle	Eccentricity	f_{bo}/f_{co}	K_c	Viscosity Parameter
10	0.1	1.16	0.667	0.0001

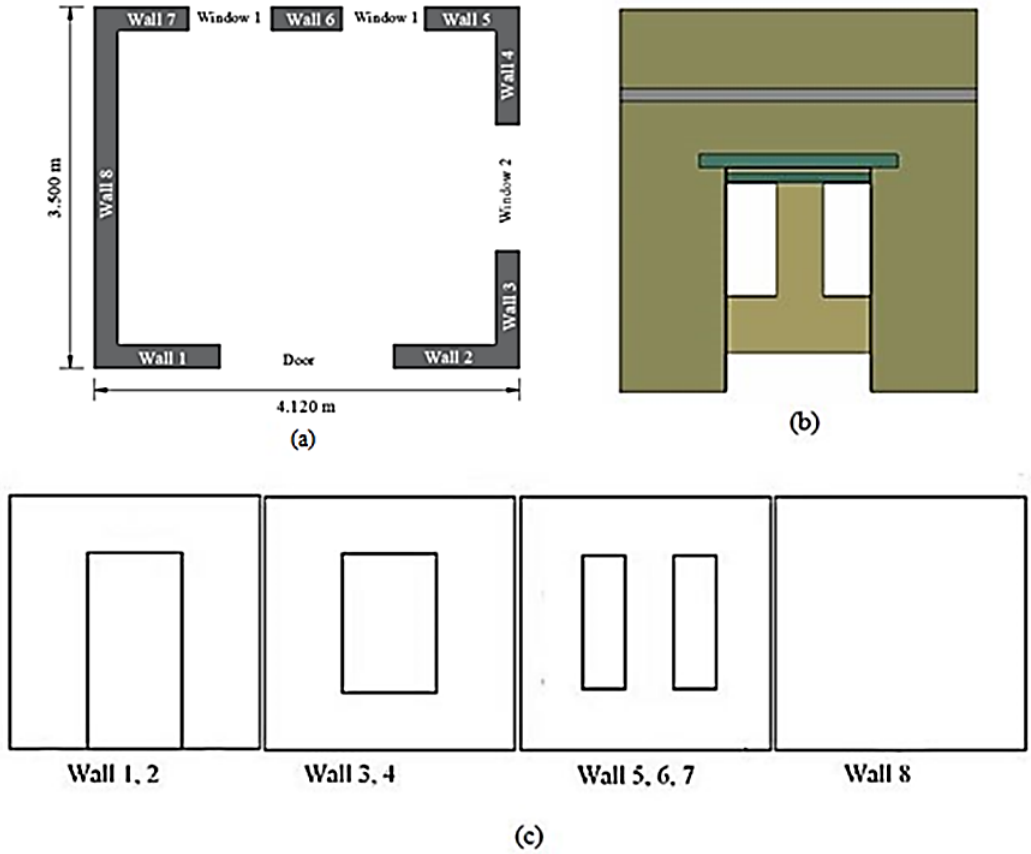

Figure 8. *Building geometry (a) Plan View, (b) 3D Model, (c) Elevation*

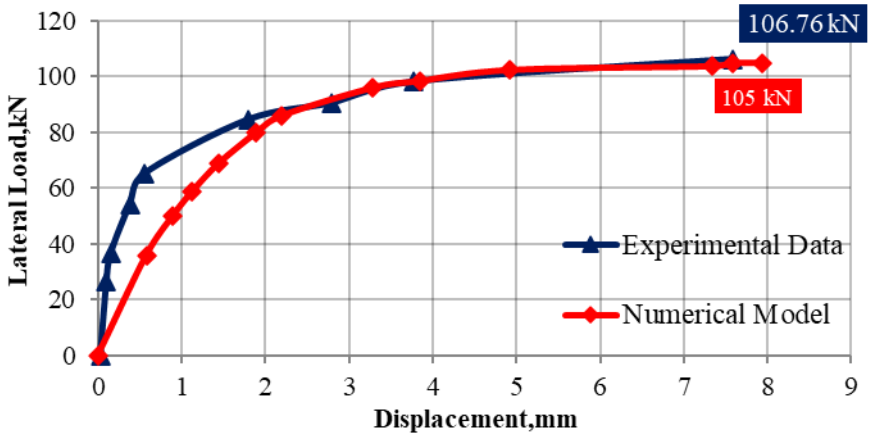

Figure 9. *Comparison of the Capacity curve with the experimental curve*

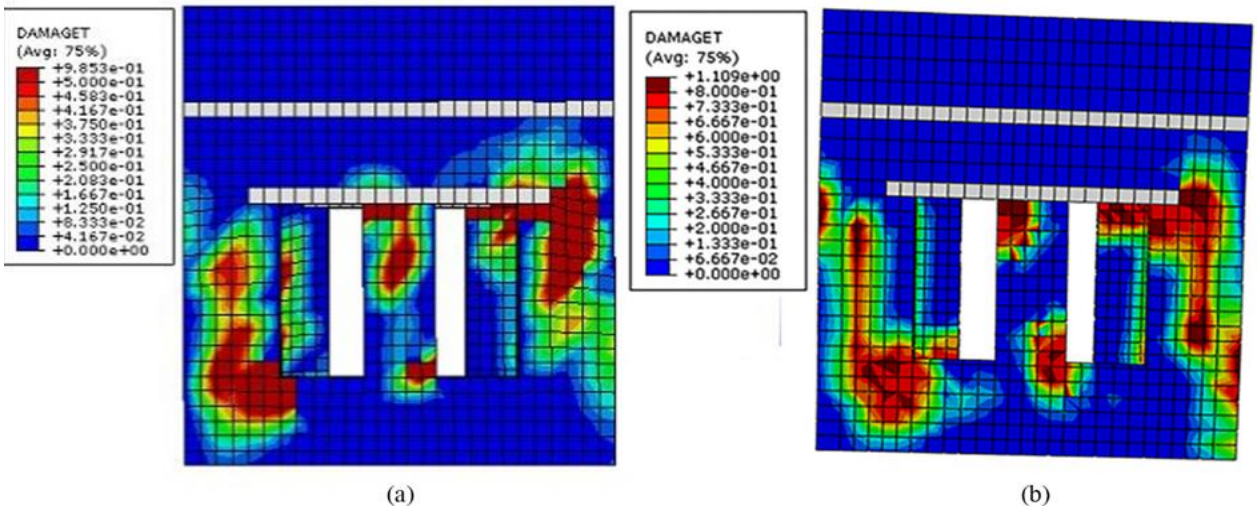

Figure 10. *Contour plots of damage in tension* ***(a)*** *Numerical Model* ***(b)*** *Literature* (Choudhury et al, 2015)

To isolate the validated masonry building model, an optimized rubber isolator is modelled between the plinth and the top beam, as shown in Figure 11. The beams have 230mm square cross sectional dimensions. The weighted score method is used to determine the dimensions of an optimized rubber isolator. An intermittent rubber-beam model with a length of 4m is used in the simulations. Using the scaling procedure, the optimized length of the rubber is obtained per metre length. If a one-meter length is taken into account, and an ideal one-story masonry wall load of 0.057Mpa is assumed, the length of the rubber is 125mm. Two walls in this building are 4.12m long and two walls are 3.5m long. The total length of rubber provided is then 515mm in the longitudinal direction and 437 in the lateral direction.

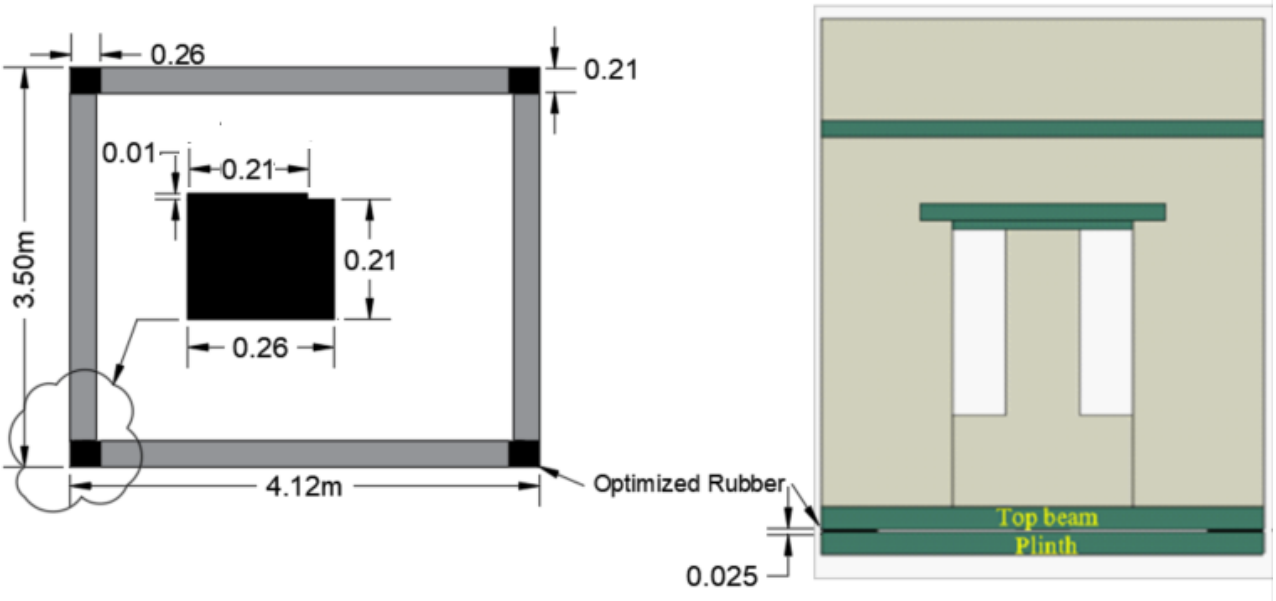

Figure 11. *Plan and elevation of building model with beams and optimized rubber (all dimensions are in m)*

Time history analysis is performed on the model with NE-Indian 1986 ground motion. The input ground motion is shown in Figure 11.

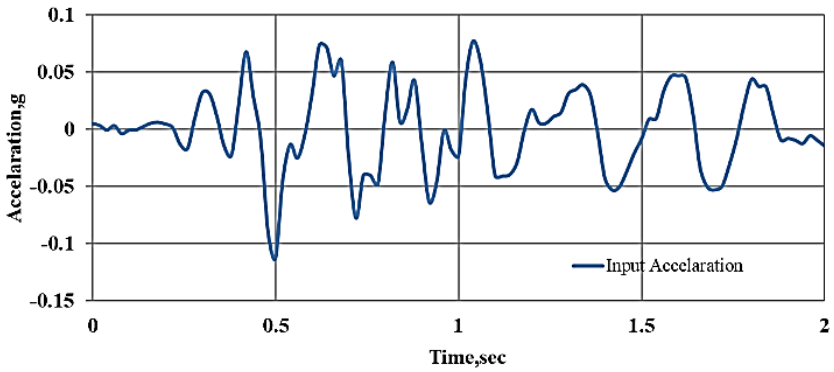

Figure 12. *Input Acceleration*

Peak acceleration at the wall-top of the model is evaluated for the Fixed Base (FB) and Base-Isolated (BI) model. There is a significant reduction in the magnitude of peak acceleration at the wall-top level. The wall-top acceleration time history plots are shown in Figure 11. Compared to building with the fixed base, the wall-top acceleration has reduced to 65%. The damage patterns of base isolated building is compared with fixed base building is shown in Figure 14. It can be observed that there is a significant reduction in the intensity of damage in tension after providing the proposed rubber isolation.

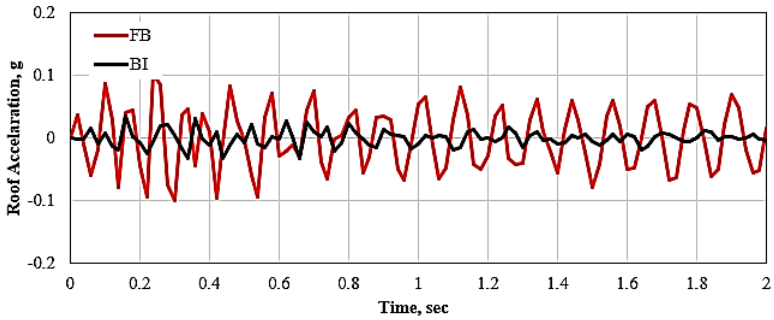

Figure 13. *Comparison of wall-top acceleration of Fixed and Isolated Building*

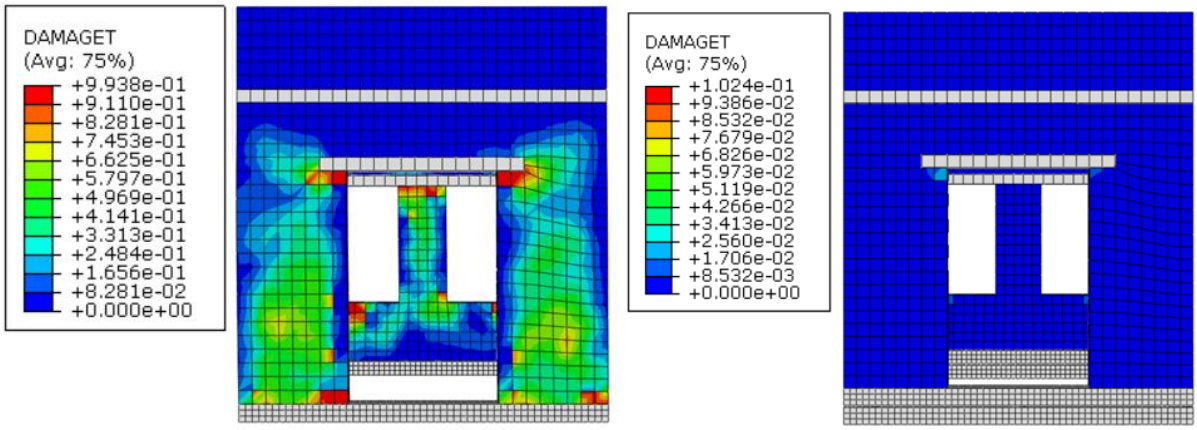

(a) (b)

Figure 14. *Comparison of damage patterns for* ***(a)*** *Fixed base and* ***(b)*** *Base isolated buildings under elcentro earthquake*

CONCLUSION

To overcome the limitations of existing isolation techniques for masonry structure, numerical analysis is performed using a novel base isolation technique. Initially, natural rubber has been used as an isolator spread throughout the wall above the plinth beam. As this did not produce satisfactory results, a gap has been created in the center of the rubber. The gap has been widened until it yielded satisfactory results. Using the results

from the numerical simulations, regression analysis is carried out to create regression models. The optimal rubber dimension is then determined using the weighted score method. A one-story masonry building, which is experimentally tested, has been used to examine the proposed technique's effectiveness. It is then hypothesized by modeling the rubber beneath the building's wall using Yeoh's coefficients and Prony's coefficient. The building is subjected to the NE-Indian 1986 earthquake. In terms of peak acceleration and damage pattern in tension, the simulation shows that the performance of base-isolated buildings has improved significantly compared to fixed base buildings. This technique is promising for the isolation of masonry buildings considering socio-economic criteria in developing countries. The obtained results are preliminary in nature and require more detailed parametric analysis and experimental validation.

REFERENCES

6.2 Friction – University Physics Volume 1. (n.d.). Retrieved December 3, 2021, from https://opentextbc.ca/universityphysicsv1openstax/chapter/6-2-friction/

Banović, I., Radnić, J., & Grgić, N. (2019). Geotechnical Seismic Isolation System Based on Sliding Mechanism Using Stone Pebble Layer: Shake-Table Experiments. *Shock and Vibration*, *2019*, 1–26. https://doi.org/10.1155/2019/9346232

Choudhury, T., Milani, G., & Kaushik, H. B. (2015). Comprehensive numerical approaches for the design and safety assessment of masonry buildings retrofitted with steel bands in developing countries: The case of India. *Construction and Building Materials*, *85*, 227–246. https://doi.org/10.1016/j.conbuildmat.2015.02.082

Coefficient of Friction Equation and Table Chart - Engineers Edge. (n.d.). Retrieved September 1, 2021, from https://www.engineersedge.com/coeffients_of_friction.htm

Das, A., Deb, S. K., & Dutta, A. (2016a). Shake table testing of un-reinforced brick masonry building test model isolated by U-FREI. *Earthquake Engineering & Structural Dynamics*, *45*(2), 253–272. https://doi.org/10.1002/eqe.2626

Das, A., Deb, S. K., & Dutta, A. (2016b). Comparison of Numerical and Experimental Seismic Responses of FREI-Supported Un-reinforced Brick Masonry Model Building. *Journal of Earthquake Engineering*, *20*(8), 1239–1262. https://doi.org/10.1080/13632469.2016.1140098

Forcellini, D. (2020). Assessment of Geotechnical Seismic Isolation (GSI) as a Mitigation Technique for Seismic Hazard Events. *Geosciences*, *10*(6), 222. https://doi.org/10.3390/geosciences10060222

Habieb, A. B., Milani, G., & Tavio, T. (2018). Two-step advanced numerical approach for the design of low-cost unbonded fiber reinforced elastomeric seismic isolation systems in new masonry buildings. *Engineering Failure Analysis*, *90*(February), 380–396. https://doi.org/10.1016/j.engfailanal.2018.04.002

Dezfuli, F. H., & Alam, M. S. (2013). Multi-criteria optimization and seismic performance assessment of carbon FRP-based elastomeric isolator. Engineering structures, 49, 525-540. https://doi.org/10.1016/j.engstruct.2012.10.028

Hwang, C. L., Masud, A., Paidy, S. R., & Yoon, K. (1979). *Multiple Objective Decision Making — Methods and Applications*. *164*. https://doi.org/10.1007/978-3-642-45511-7

Karimzadeh Naghshineh, A., Akyüz, U., & Caner, A. (2014). Comparison of fundamental properties of new types of fiber-mesh-reinforced seismic isolators with conventional isolators. *Earthquake Engineering & Structural Dynamics*, *43*(2), 301–316. https://doi.org/10.1002/EQE.2345

Kelly, J. (1999). Analysis of Fiber-Reinforced Elastomeric Isolators. *Journal of Seismology and Earthquake Engineering*, *2*(1), 19–34.

Minke, G. (1984). Earthquake resistant low-cost houses utilizing indigenous building materials and intermediate technology. In Earthquake relief in less industrialized areas. I*nternational symposium organized by the swiss national committee for earthquake engineering zurich 28/30 march 1984* (pp. 105-108).

Mishra, H. K., Igarashi, A., & Matsushima, H. (2013). Finite element analysis and experimental verification of the scrap tire rubber pad isolator. *Bulletin of Earthquake Engineering*, *11*(2), 687–707. https://doi.org/10.1007/s10518-012-9393-4

Nanda, R. P., Shrikhande, M., & Agarwal, P. (2016). Low-Cost Base-Isolation System for Seismic Protection of Rural Buildings. *Practice Periodical on Structural Design and Construction*, *21*(1), 04015001. https://doi.org/10.1061/(asce)sc.1943-5576.0000254

Osgooei, P. M., Tait, M. J., & Konstantinidis, D. (2014). Finite element analysis of unbonded square fiber-reinforced elastomeric isolators (FREIs) under lateral loading in different directions. *Composite Structures*, *113*(1), 164–173. https://doi.org/10.1016/j.compstruct.2014.02.033

Russo, G., & Pauletta, M. (2013). Sliding instability of fiber-reinforced elastomeric isolators in unbonded applications. *Engineering Structures*, *48*, 70–80. https://doi.org/10.1016/j.engstruct.2012.08.031

Russo, G., Pauletta, M., & Cortesia, A. (2013). A study on experimental shear behavior of fiber-reinforced elastomeric isolators with various fiber layouts, elastomers and aging conditions. *Engineering Structures*, *52*, 422–433. https://doi.org/10.1016/j.engstruct.2013.02.034

Shahzada, K., Khan, A. N., Elnashai, A. S., Ashraf, M., Javed, M., Naseer, A., & Alam, B. (2012). Experimental seismic performance evaluation of unreinforced brick masonry buildings. *Earthquake Spectra*, *28*(3), 1269–1290. https://doi.org/10.1193/1.4000073

Sierra, I. E. M., Casas, J. M., & Thomson, P. (2019a). Matrix and reinforcement materials for low-cost building isolators: An overview of results from experimental tests and numerical simulations. *Journal of Applied Research and Technology*, *17*(1), 44–56. https://doi.org/10.22201/icat.16656423.2019.17.1.756

Sierra, I. E. M., Losanno, D., Strano, S., Marulanda, J., & Thomson, P. (2019b). Development and experimental behavior of HDR seismic isolators for low-rise residential buildings. *Engineering Structures*, *183*(January), 894–906. https://doi.org/10.1016/j.engstruct.2019.01.037

Spizzuoco, M., Calabrese, A., & Serino, G. (2014). Innovative low-cost recycled rubber-fiber reinforced isolator: Experimental tests and Finite Element Analyses. *Engineering Structures*, *76*, 99–111. https://doi.org/10.1016/j.engstruct.2014.07.001

Thuyet, V. N., Deb, S. K., & Dutta, A. (2018). Mitigation of Seismic Vulnerability of Prototype Low-Rise Masonry Building Using U-FREIs. *Journal of Performance of Constructed Facilities*, *32*(2), 1–13. https://doi.org/10.1061/(ASCE)CF.1943-5509.0001136

Toopchi-Nezhad, H. (2014). Horizontal stiffness solutions for unbonded fiber reinforced elastomeric bearings. *Structural Engineering and Mechanics*, *49*(3), 395–410. https://doi.org/10.12989/sem.2014.49.3.395

Toopchi-Nezhad, Hamid, Tait, M. J., & Drysdale, R. G. (2008a). Lateral Response Evaluation of Fiber-Reinforced Neoprene Seismic Isolators Utilized in an Unbonded Application. *Journal of Structural Engineering*, *134*(10), 1627–1637. https://doi.org/10.1061/(asce)0733-9445(2008)134:10(1627)

Toopchi-Nezhad, Hamid, Tait, M. J., & Drysdale, R. G. (2008b). Testing and modeling of square carbon fiber-reinforced elastomeric seismic isolators. *Structural Control and Health Monitoring*, *15*(6), 876–900. https://doi.org/10.1002/stc.225

Toopchi-Nezhad, Hamid, Tait, M. J., & Drysdale, R. G. (2011). Bonded versus unbonded strip fiber reinforced elastomeric isolators: Finite element analysis. *Composite Structures*, *93*(2), 850–859. https://doi.org/10.1016/j.compstruct.2010.07.009

Tran, C., Calabrese, A., Vassiliou, M. F., & Galano, S. (2020). A simple strategy to tune the lateral response of unbonded Fiber Reinforced Elastomeric Isolators (FREIs). *Engineering Structures*, *222*(June), 111128. https://doi.org/10.1016/j.engstruct.2020.111128

Tsiavos, A., Alexander, N. A., Diambra, A., Ibraim, E., Vardanega, P. J., Gonzalez-Buelga, A., & Sextos, A. (2019). A sand-rubber deformable granular layer as a low-cost seismic isolation strategy in developing countries: Experimental investigation. *Soil Dynamics and Earthquake Engineering*, *125*(June), 105731. https://doi.org/10.1016/j.soildyn.2019.105731

Tsiavos, A., Sextos, A., Stavridis, A., Dietz, M., Dihoru, L., & Alexander, N. A. (2020). Large-scale experimental investigation of a low-cost PVC 'sand-wich' (PVC-s) seismic isolation for developing countries. *Earthquake Spectra*, *36*(4), 1886–1911. https://doi.org/10.1177/8755293020935149

Turer, A., & Özden, B. (2008). Seismic base isolation using low-cost Scrap Tire Pads (STP). *Materials and Structures/Materiaux et Constructions*, *41*(5), 891–908. https://doi.org/10.1617/s11527-007-9292-3

Vaiana, N., Sessa, S., Marmo, F., & Rosati, L. (2019). An accurate and computationally efficient uniaxial phenomenological model for steel and fiber reinforced elastomeric bearings. *Composite Structures*, *211*(August 2018), 196–212. https://doi.org/10.1016/j.compstruct.2018.12.017

Van Engelen, N. C., Osgooei, P. M., Tait, M. J., & Konstantinidis, D. (2015). Partially bonded fiber-reinforced elastomeric isolators (PB-FREIs). *Structural Control and Health Monitoring*, *22*(3), 417–432. https://doi.org/10.1002/stc.1682

Yoon, K. P., & Hwang, C. L. (1995). Multiple Attribute Decision Making: An Introduction, Sage, Thousand Oaks, CA. *Sage Publications Thousand Oaks CA*, *104*, 75. p. 38.